J Solid State Electrochem (2016) 20:2009–2018
DOI 10.1007/s10008-016-3201-z

ORIGINAL PAPER

Highly catalytic activity of platinum-gold particles modified poly(*p*-aminophenol) electrode for oxygen reduction reaction

Şükriye Ulubay Karabiberoğlu[1] · **Zekerya Dursun**[1]

Received: 19 December 2015 / Revised: 24 March 2016 / Accepted: 29 March 2016 / Published online: 13 April 2016

Abstract A highly active electrocatalyst has been developed based on poly(*p*-aminophenol) polymer film modified with Pt-Au bimetallic particles on a glassy carbon electrode (Pt-Au/PPAP/GCE) for electrocatalytic reduction of oxygen. The surface morphology and chemical analyses of the modified electrodes have been revealed by scanning electron microscopy (SEM), transmission electron microscopy (TEM), energy-dispersive X-ray spectroscopy (EDX), and electrochemical impedance spectroscopy (EIS). The Pt-Au/PPAP/GCE has shown the best electrocatalytic activity towards O_2 reduction in comparison to the other used electrodes. The rotating disk electrode (RDE) studies have indicated that the oxygen reduction reaction takes place via almost four electrons on the Pt-Au/PPAP/GCE.

Keywords Oxygen reduction · Platinum-gold particles · Polymer film · Fuel cell

Introduction

Higher catalytic active surfaces for both cathodic and anodic compartments have been extensively studied in order to develop an effective energy converter system in fuel cells. The electrochemical reduction of oxygen is an important reaction not only for electrochemical energy systems but also for industrial process, e.g., hydrogen peroxide synthesis, metal-air batteries, and gas sensors [1–4]. The pathway of oxygen reduction reaction is greatly influenced by the supporting electrolyte and the electrode material composition [5–7]. The most efficient pathway is direct four-electron reduction of molecular oxygen to water. Two-electron reduction process at two different potentials on bare electrode surface is reported to be a less efficient pathway [8–10]. The sluggish kinetics and thereby the high overpotentials for oxygen reduction reaction (ORR) have enabled the current uses of noble metals such as platinum, palladium, and bimetallic/intermetallic compositions as the electrocatalysts to accelerate the reduction kinetics [11–13]. Generally, platinum and other precious metals have been widely used to accelerate the kinetics of the ORR in fuel cell applications as electrocatalysts [14–18]. These materials show high electrocatalytic activity with a high cost. Therefore, researchers have been focused to find out alternative catalyst materials in order to solve high cost disadvantages. Recently, precious metal-free materials have been studied for the reduction of oxygen, but only a few materials (copper, cobalt, manganese, etc.) showed electrocatalytic activity towards this reaction with an unstable surface [4, 9, 19–21]. The second option to minimize high cost problems is to use a small amount of metal particles of precious metals. The bimetallic formation of Au and Pt particle-modified electrodes have shown higher electrocatalytic activity for both reduction of oxygen molecule and oxidation of many organic and inorganic compounds by keeping their own properties in the presence of electroactive compounds and supporting electrolytes. In addition to this, oxygen reduction can be observed by transferring four electrons on bulk Pt catalysts. The positive electrocatalytic effect towards oxygen reduction reaction can be obtained with Au-Pt metallic surface due to synergetic effect between Au and Pt [22–26].

✉ Şükriye Ulubay Karabiberoğlu
sukriyeulubay@gmail.com

✉ Zekerya Dursun
zekerya.dursun@ege.edu.tr

[1] Department of Chemistry, Faculty of Science, Ege University, 35100 Bornova, Izmir, Turkey

Metal particles on the surface of the bare electrode are fragile and can easily be agglomerated. To overcome this problem, the bare electrode surface is covered with some stabilizing porous substances such as carbon nanotubes and conductive polymers and then the metal particles are deposited on the modified electrode surfaces. At this point, the porous structure of the conducting polymer, nanotubes, or other conductive materials provide a homogeneous dispersion of the metal particles on the surface and constitute adjunct electrocatalytic sites [14, 27]. Metal particle-modified conducting polymer film electrodes have been studied for electrocatalytic applications in oxygen reduction reaction. The performance of the electrocatalytic activity of the modified metal-polymer composite structures such as carbon supported Co-polypyrrole film electrode [28], platinum deposited poly(4-amino-3-hydroxynaphthalene sulfonic acid) GCE [14], gold nanoparticles dispersed into poly(aminothiophenol) film electrode [29], Pt dispersed on chemically prepared poly(3,4-ethylenedioxythiophene)/poly(styrene-4-sulfonate) film electrode [30], poly(*p*-aminobenzene sulfonic acid)-modified glassy carbon electrode [31], $Cu_xMn_{3-x}O_4$ particles modified polypyrrole composite electrode [32] were enhanced. To our knowledge, the electrochemical reduction of oxygen on Au-Pt bimetallic particle-modified poly(*p*-aminophenol) composite electrode has not been reported yet.

In the present study, the electrocatalytic activity of Pt-Au bimetallic particles modified poly(*p*-aminophenol) composite electrode (Pt-Au/PPAP/GCE) was used for oxygen reduction in alkaline solutions. Au and Pt metal particles were generated ex situ on poly(*p*-aminophenol) film-modified GCE with cyclic voltammetry (CV). The characterization of these electrodes was performed by using SEM, TEM, EDX, and EIS. The electrocatalytic activity of bimetallic particle-modified Pt-Au/PPAP/GCE towards oxygen reduction reaction (in 0.1 M NaOH solution) was also compared with bare GC, PPAP/GC, monometallic Au, and Pt particle-modified PPAP/GC electrodes.

Experimental

Reagents

The *p*-aminophenol and sodium dodecyl sulfate (SDS) were purchased from Sigma. NaOH used as an electrolyte was obtained from Raidel De Haen. HNO_3, HCl, and $HClO_4$ were all in ultra-pure grade, purchased from Merck. Chloroauric acid solution was prepared by dissolving Au wire (99.999 % in purity, Tanaka Kikinzoku Kogyo Co., Ltd.) in a mixture of concentrated HNO_3/HCl (volume ratio of 1:3). K_2PtCl_6 was purchased from Sigma and used to prepare solutions for the Pt particle formation on PPAP/GCE. All solutions were prepared using ultra-pure water (Milli-Q 18.2 MΩ cm, Millipore System Inc.). All experiments were performed in an oxygen-free solution under high-purity N_2 gas atmosphere.

Apparatus

Voltammetric measurements were carried out using a BAS 100B/W voltammetric analyzer (Bioanalytical Systems, Inc.) including three-electrode system. Depending on the specific test, various stationary or rotating disk electrodes were used as working electrodes, such as bare GCE, PPAP/GCE, Au/PPAP/GCE, Pt/PPAP/GCE, and Pt-Au/PPAP/GCE. In the present study, a platinum wire was used as the auxiliary electrode and Ag/AgCl sat.KCl were preferred as the reference electrode. Electrochemical impedance measurements were realized by Autolab 302N. The SEM/EDX measurements were performed using the Phillips XL-30S for the characterization of polymer film and metal particles on the electrode surfaces. Transmission electron microscopic (TEM) images were obtained using a JEOL JEM-2100 microscope. X-ray photoelectron spectroscopy (XPS) spectra of the bimetallic Pt-Au particles deposited on PPAP/GC electrodes were collected via a Thermo Scientific spectrometer with K-Alpha surface analysis.

Preparation of poly(*p*-aminophenol)-modified glassy carbon electrode

The GCE was polished with Al_2O_3 slurry and then sonicated subsequently in a 1:1 ultra-pure water and ethanol for 5 min, respectively. The poly(*p*-aminophenol) film on the GCE surface has been formed using cyclic voltammetry by changing current-potential cycling number in the presence of 0.5 mol L^{-1} aqueous $HClO_4$ solution containing 5.0 mmol L^{-1} PAP in the presence of 5.0 mmol L^{-1} SDS. The obtained PPAP/GCE was rinsed with distilled water several times to remove the remaining PAP adsorbed on the surface of the electrode [33, 34].

Preparation of Pt-Au-doped poly(*p*-aminophenol) -modified glassy carbon electrode

The electrochemical deposition of Au and Pt metal particles were performed by using cyclic voltammetry in 1.0 mmol L^{-1} $HAuCl_4$ and K_2PtCl_6 on the PPAP/GCE in 0.10 mol L^{-1} HCl solution. The electrodeposition of Au and Pt particles was carried out by increasing current-potential cycling number. The potential scan was started from 0.10 to −0.90 V for cathodic scan and from −0.90 to 0.10 V for anodic scan for Au deposition, whereas the scan was made from 0.80 to −0.90 V for cathodic scan and from −0.90 to 0.80 V for anodic scan for Pt deposition.

Results and discussion

Preparation of the modified electrodes

The consecutive cyclic voltammograms of *p*-aminophenol (PAP) for electropolymerization on GCE have shown a good agreement with previous works [33, 34]. An anionic dopant, SDS, was used to increase the conductivity of polymer. Figure 1a shows the consecutive CVs for the preparation of Au particles in 1.0 mmol L^{-1} $HAuCl_4$ + 0.1 mol L^{-1} HCl on the PPAP/GCE in the potential range of 0.1 to −0.9 V at 50 mV s^{-1} for 10 cycles. In the first cycle, a reduction peak has appeared at −0.5 V corresponding to the reduction of Au^{3+} ions to Au^0. The peak currents increased depending on the current-potential cycle number. Pt particle-modified Au/PPAP/GC electrode was prepared in 1.0 mmol L^{-1} K_2PtCl_6 + 0.1 mol L^{-1} HCl by the same method in the potential range of 0.8 to −0.9 V (Fig. 1b). Two reduction peaks of Pt^{4+} ions have appeared at −0.2 and −0.8 V corresponding to the reduction of Pt^{4+} ions to Pt^0 via a two-step reduction reaction. The peak currents of reduction peaks have not changed as cycle number increased. Finally, Pt-Au/PPAP/GC electrodes were obtained using the procedure mentioned above.

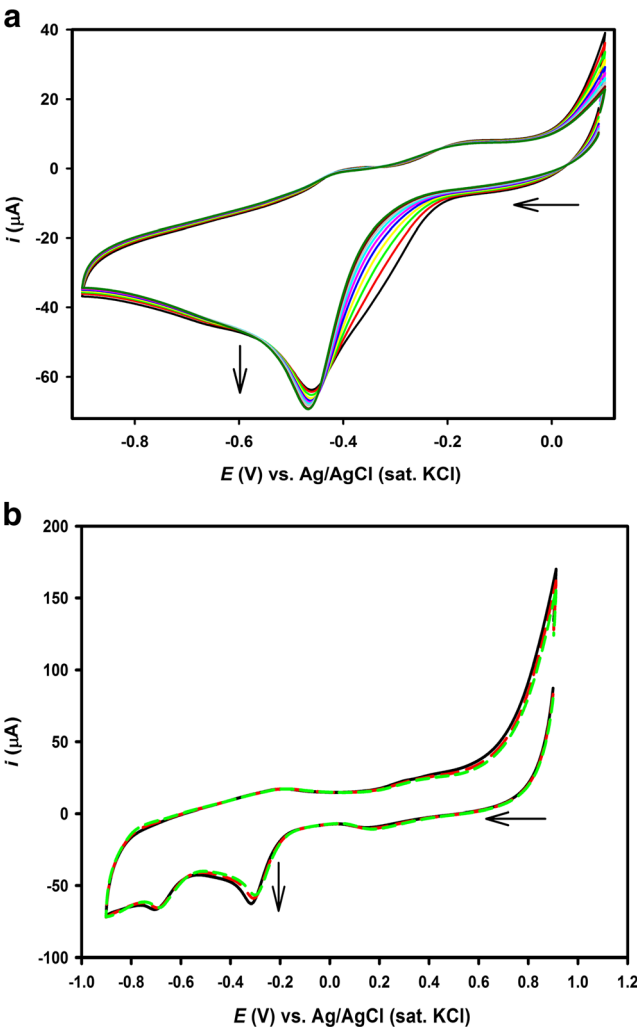

Fig. 1 The PPAP/GC electrode modified with **a** Au particles in N_2-saturated 1.0 mmol L^{-1} $HAuCl_4$ and **b** Au/PPAP/GC electrode modified with Pt particles in 1.0 mmol L^{-1} K_2PtCl_6 by repeating the potential scan at 0.05 V s^{-1} for ten cycles

Evaluation of electroactive surface area

The electroactive surface areas of the working electrodes (GCE, PPAP/GCE, Au/PPAP/GCE, Pt/PPAP/GCE, Au-Pt/PPAP/GCE, and Au-Pt/GCE) were obtained by the measurement of the peak current at a different scan rate using the Randles-Sevcik equation using cyclic voltammetry in 1.0 mmol L^{-1} $K_4Fe(CN)_6$ + 0.1 mol L^{-1} KCl solution [35, 36]. The dependence of peak current I_p on the scan rate $\nu^{1/2}$ is described by the Randles-Sevcik equation:

$$I_p = \left(2.69 \times 10^5\right) n^{3/2} A D^{1/2} C^* \nu^{1/2} \quad (1)$$

where n represents the number of electrons participating in the redox reaction, ν is the scan rate of the potential perturbation (V/s), A is the area of the electrode (cm^2), D is the diffusion coefficient of the molecules in the solution (cm^2/s), C^* is the concentration of the probe molecule in the bulk solution (mol cm^{-3}), and I_p is the peak current of the redox couple. In the equation, the effective surface area (A) can be calculated from the value of $I_p/\nu^{1/2}$ since D, n (n = 1), and C^* (1.0 mmol L^{-1}) are constant values. The diffusion constant value at 25 °C ($D = 6.7 \times 10^{-5}$ cm^2 s^{-1}) was obtained from the literature data [37]. At all electrodes, the I_p increases linearly with the increasing of the square root of the potential scan rate ($\nu^{1/2}$), which suggests that the reactions occurring on the modified electrode were nearly reversible. From the slope of the linear graph, the electroactive areas of the GCE, PPAP/GCE, Au/PPAP/GCE, Pt/PPAP/GCE, Pt-Au/PPAP/GCE, and Au-Pt/GCE were calculated to be 0.056, 0.075, 0.101, 0.062, 0.230, and 0.077 cm^2, respectively. Obviously, when the glassy carbon electrode surface was modified with polymer and metal nanoparticles, the electroactive surface area increases and hence the electron transfer was promoted for oxygen reduction which proved increasing of peak current and positively shifting of oxygen reduction potential.

Characterization of the modified electrodes

Figure 2 shows the SEM images of bare GCE, PPAP/GCE, and PPAP/GCEs modified with Au and Pt metal particles. A smoother electrode surface obtained at bare GCE is observed (Fig. 2a). The formation of PPAP was noticed on the electrode surface (Fig. 2b). As seen in Fig. 2c, d, bright Au particles and Pt particles were formed, were dispersed homogeneously, and were decorated to the polymer film electrode surface. Figure 2e shows the SEM image of PPAP/GCE after Pt-Au

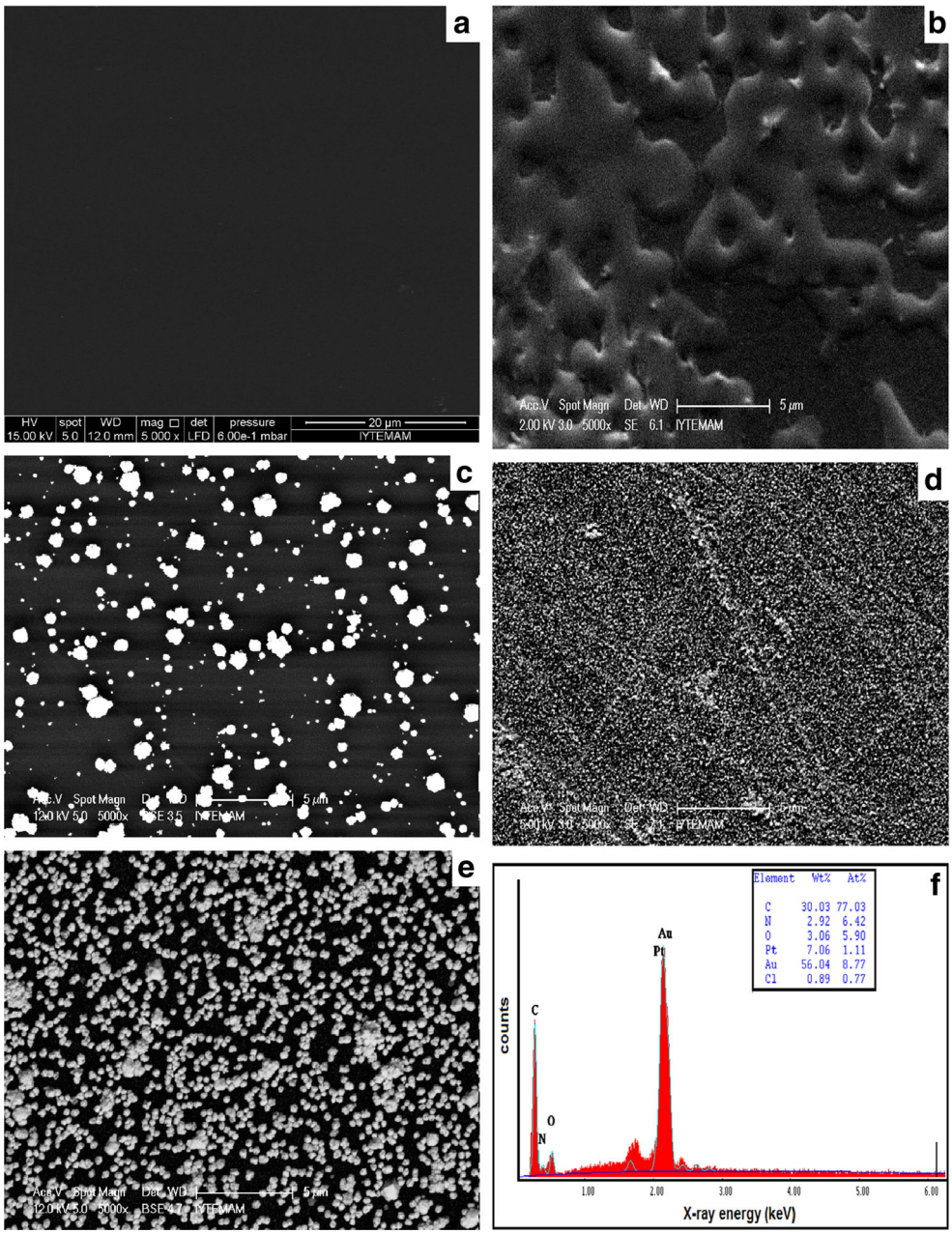

Fig. 2 SEM images of the **a** bare GCE, **b** PPAP/GCE, **c** Au/PPAP/GCE, **d** Pt/PPAP/GCE, **e** Pt-Au/PPAP/GCE, and **f** EDX image of Pt-Au/PPAP/GCE

electrodeposition. A typical EDX spectrum obtained from the surface of Pt-Au/PPAP/GC electrode was presented in Fig. 3f which confirmed the presence of Au and Pt particles decorated on PPAP/GCE.

Figure 3 shows the TEM image of the Pt-Au/PPAP composite, which clearly demonstrates that the formed Pt-Au particles were dispersed as roughly in a spherical and triangular shape in diameters ranging from 15 to 25 nm as shown in Fig. 3. On the other hand, comparison of SEM and TEM images indicated that the metal particles' diameter was not the same due to the dissimilar preparation of SEM and TEM sample procedures. In the SEM measurements, the electrochemically prepared modified surface can be directly monitored by the SEM system without any additional operation, so the original electrode surface was protected. But in the case of TEM measurements, after the electrochemically prepared modified surface with in both polymers and metal particles, the content had to be scraped from the electrode surface with a sharp knife and transferred to ethanol solution and then TEM grids. During the TEM sample preparation steps, the metal particles could be released to the small particles compared to SEM conditions. Therefore, the metal particles' size in SEM images was higher than that in the TEM images.

Figure 4a–c shows the XPS spectra of Pt4f of Pt/PPAP/GCE, Au4f of Au/PPAP/GCE, and Pt4f and Au4f of Au-Pt/PPAP/GCE that prepared consequently deposition of Au and

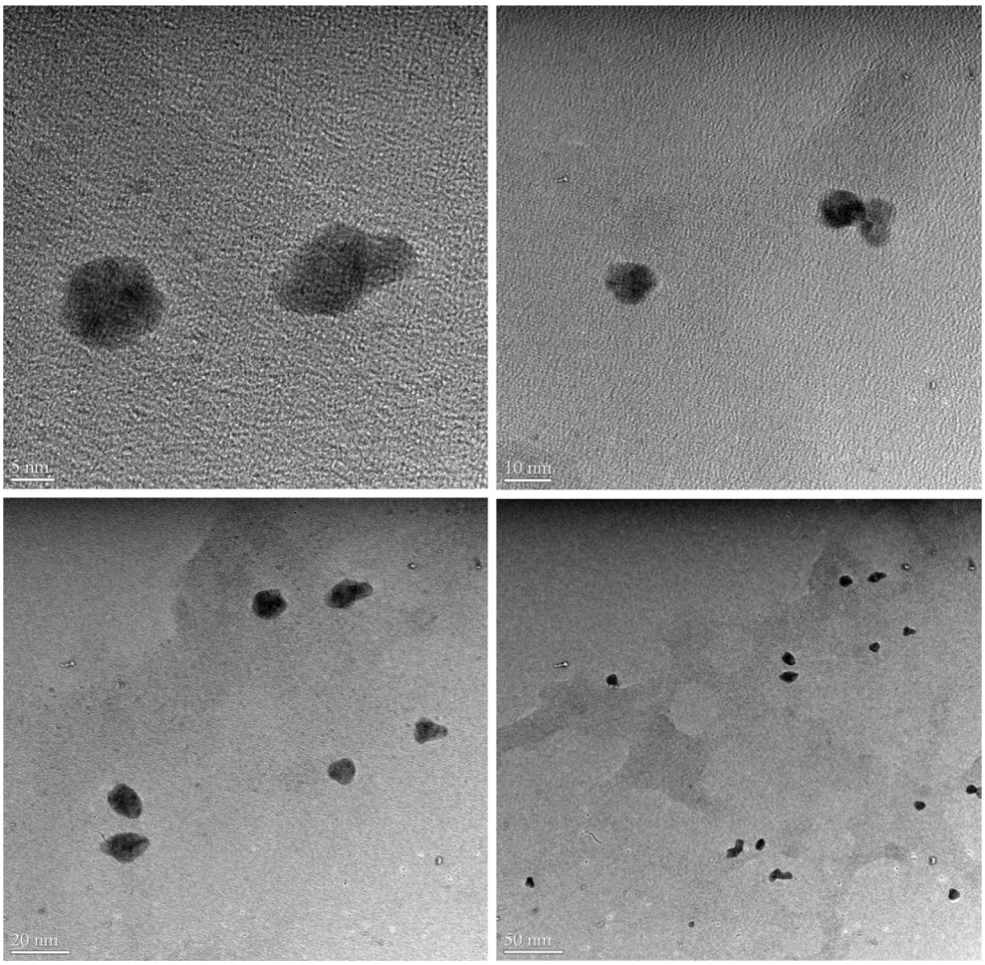

Fig. 3 TEM images of Pt-Au/PPAP in various magnifications

Pt, respectively. The Pt4f signal of both Pt/PPAP and Pt-Au/PPAP electrodes shows two doublet peaks due to spine orbital splitting of the $4f_{7/2}$ and $4f_{5/2}$ states, as displayed in Fig. 4a, c. The two relative intense doublet peaks with binding energies of 71.18 and 71.08 eV on Pt/PPAP and Pt-Au/PPAP ($Pt4f_{7/2}$) and 74.58 and 74.78 eV on Pt/PPAP and Pt-Au/PPAP ($Pt4f_{5/2}$), respectively, should be attributed to the metallic Pt [25].Therefore, it is suggested that the Pt particles have been obtained in metallic forms. Figure 4b, c shows the Au4f spectrum resolved into two spin-orbit components ($Au4f_{7/2}$ and $4f_{5/2}$) on Au/PPAP and Pt-Au/PPAP electrodes. The doublet peaks occurred at 84.33 and 84.08 eV on Au/PPAP and Pt-Au/PPAP electrodes ($Au4f_{7/2}$); 87.78 and 87.88 eV on Au/PPAP and Pt-Au/PPAP electrodes ($Au4f_{5/2}$) were assigned to metallic Au [29] and Pt [25].

The binding energy of Au and Pt in the bimetallic conditions was shifted compared with Au and Pt metal particle-modified PPAP/GCE values alone. The energy separation of species in all electrodes were proved as their metallic forms. But the shifts of binding energy values were observed due to the alloy formation with atomic level mixing of Pt and Au deposition.

Figure 5 illustrates the results of electrochemical impedance spectroscopy (EIS) on bare GCE, PPAP/GCE, Au/PPAP/GC, and Pt/PPAP/GC and Pt-Au/PPAP/GC in the presence of 5.0 mmol L^{-1} $K_3[Fe(CN)_6]/K_4[Fe(CN)_6]$ containing 0.1 mol L^{-1} KNO_3 solution at varying frequencies from 0.15 to 75,000 Hz. It can be seen that all electrodes represent a semi-circular and linear portion. The semi-circle corresponds to the charge transfer process through the GCE and polymer films at high frequencies, whereas the second one was due to the diffusion process in the low frequencies. The diameter of the semi-circle represents the magnitude of electron-transfer resistance at the electrode surface. The obtained EIS data were fitted with an equivalent circuit as given in Fig. 5 inset. This equivalent circuit consists of the ohmic resistance (R_s) of the electrolyte solution, the double layer capacitance (C_{dl}), and the electron-transfer resistance (R_{ct}) resulting from the diffusion of ions from the bulk of the electrolyte to the interface. This equivalent circuit was used to fit the impedance spectra and extract the values of R_{ct} (Fig. 5 inset). The R_{ct} for the bare GCE is 559 Ω, which was higher than the R_{ct} values obtained for PPAP/GCE (360 Ω). The R_{ct} values of Au/PPAP/GC and Pt/PPAP/GC electrodes are 287 and 280 Ω, respectively. The

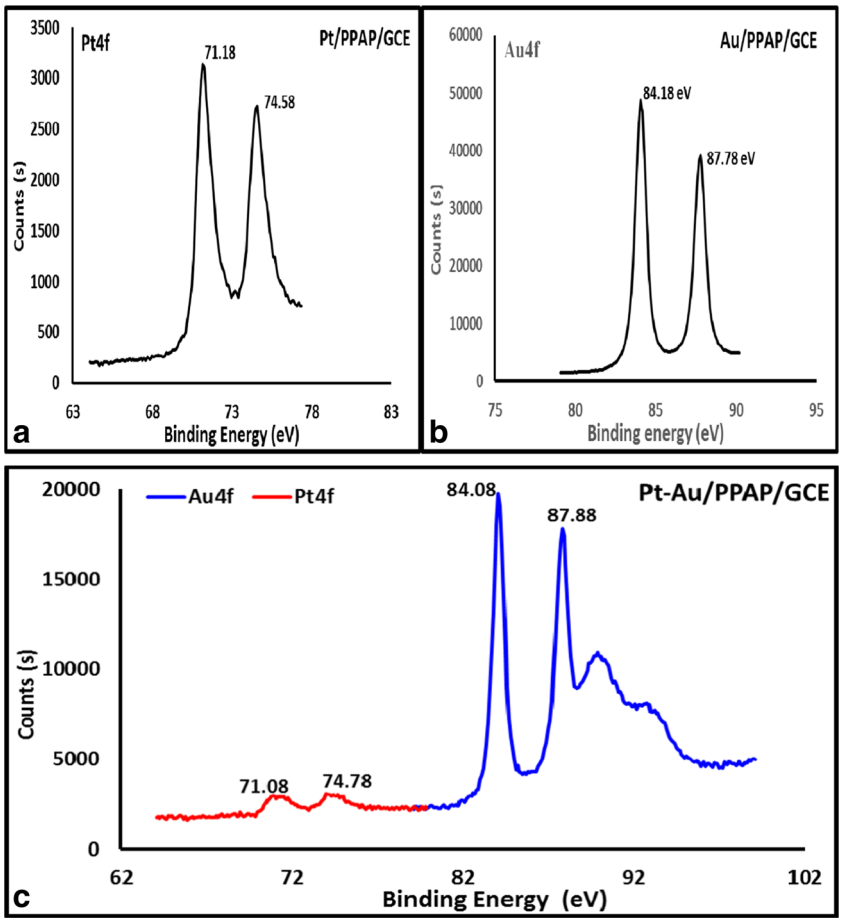

Fig. 4 Pt_{4f} XPS spectra (**a**) and Au_{4f} XPS spectra (**b**) of Au-Pt/PPAP/GCE

R_{ct} values of Pt-Au bimetallic surface were obviously decreased (187 Ω). This phenomenon indicated the excellent electroconductibility of Pt-Au bimetallic surface. Moreover, the Pt-Au/PPAP film was successfully formed on the GCE surface [38–40]. These results obtained from EIS were in agreement with standard Randles equivalent-model circuit in the high-frequency range (inset of Fig. 5). This low R_{ct} value for Pt-Au/PPAP/GCE implies that the charge transfer process is relatively fast when compared to all other electrodes.

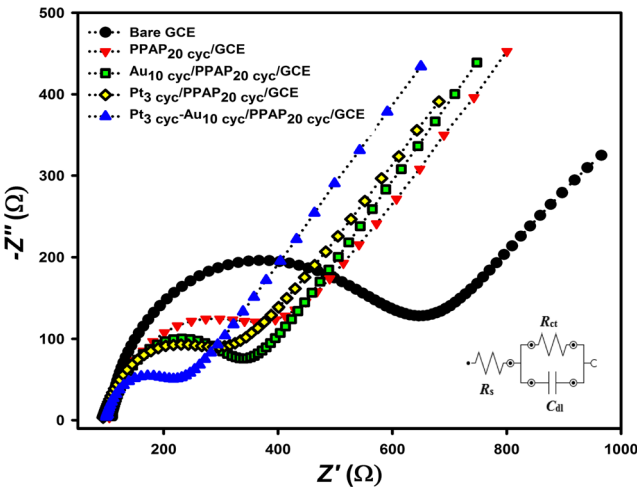

Fig. 5 The Nyquist plots of AFM images of the (*black circle*) bare GCE, (*black inverted triangle*) PPAP/GCE, (*black square*) Au/PPAP/GCE, (*black diamond*) Pt/PPAP/GCE, and (*black triangle*) Pt-Au/PPAP/GCEin 5.0 mmol L^{-1} $Fe(CN)_6^{3-}/Fe(CN)_6^{4-}$ (1:1) solution containing 0.1 mol L^{-1} KCl. The frequency range was from 0.15 to 75,000 Hz at the formal potential about 0.22 V

Electrocatalytic reduction of oxygen

The linear voltammograms of oxygen reduction (0.1 mol L^{-1} NaOH with O_2 saturated solution) on bare GCE and modified electrodes were given in Fig. 6. The peak potential of oxygen reduction was observed at −0.56 and −0.45 V on bare GC and PPAP/GC electrodes, respectively. Moreover, the peak current of oxygen reduction on PPAP/GCE was 2.5 times higher than bare GCE due to the increase of active surface area. A broad peak for oxygen reduction has appeared at bare GCE due to the slow electron transfer at the electrode surface in alkaline media. On the contrary, a prominent peak appearing at the PPAP/GCE indicates a fast electron transfer. In order to increase the electrocatalytic activity of polymer film electrode towards oxygen reduction, Pt-Au bimetallic particle-modified PPAP/GCE was prepared and used for oxygen reduction reaction in 0.1 mol L^{-1} NaOH solution. The performance of Pt-

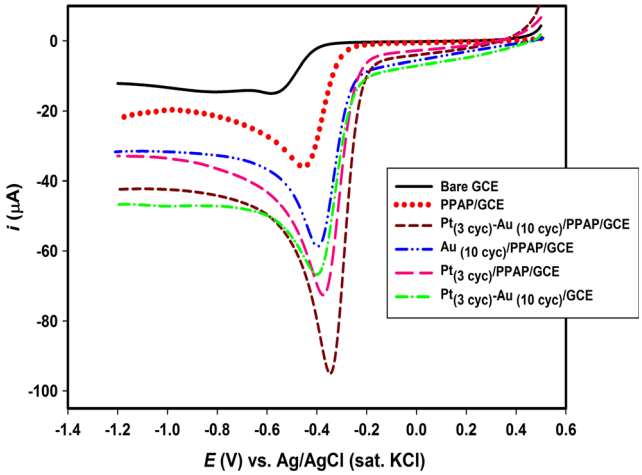

Fig. 6 Linear voltammetric behavior of bare GCE, PPAP/GCE, and different metal particles modified PPAP/GC electrodes (**a**) and Pt-Au/PPAP/GCE, bare GCE, and Pt disk electrode (**b**) in O_2 saturated 0.1 mol L^{-1} NaOH with 50.0 mV s^{-1}

Au bimetallic particle-modified PPAP/GCE to oxygen reduction was found to be very effective when compared to the bare GCE and other modified electrodes. The peak current of oxygen reduction on Pt-Au/PPAP/GCE is higher 6.2 and 3.1 times than bare GCE and PPAP/GCE, respectively. Moreover, the peak potential of oxygen reduction on Pt-Au/PPAP/GCE has shifted about 0.22 and 0.10 V in positive directions, for GCE and PPAP/GCE, respectively. As can be seen from these results, the presence of the Au-Pt bimetallic surface plays a great role, providing an advantageous and high-performance electrode for the reduction of oxygen with a faster electron transfer. It can be concluded that the synergistic effect of these bimetallic particles takes place towards the electrocatalytic activity of O_2 reduction. Regarding the performance of Pt-Au/PPAP/GCE compared with the Pt-Au/GCE electrode, the reduction current increases in the presence of a polymer film. On the other hand, a higher stability was obtained for Pt-Au/PPAP/GCE compared with Pt-Au/GCE.

In our previous work [41], oxygen electrocatalytic reduction reaction has been investigated on Cu-Au particles on multiwall carbon nanotube-modified GC electrode (Cu-Au/MWCNT/GCE). The electrocatalytic activities of Cu-Au/MWCNT and Au-Pt/PPPAP-modified glassy carbon electrodes are almost the same. The oxygen reduction peaks at both electrodes is located at close potentials. On the other hand, preparation of polymer film surface is more easy than carbon nanotube-modified surface. When the stabilities of both electrodes are compared, the Pt-Au/PPAP/GC electrode is more stable for oxygen reduction reaction due to polymer film which is deposited by electrochemical procedure; carbon nanotubes are connected by the dropping method on electrode surface. The other disadvantage of carbon nanotubes is that the MWCT content on the rotating disc electrode can be easily ruptured from the surface during the electrochemical studies by rotation of the modified electrodes. The present study results were compared with published data as summarized in Table 1. As can be seen from Table 1, the catalytic activity of Pt-Au/PPAP/GCE is competing with other catalytic surfaces.

Several parameters including monomer concentration, polymerization cycle number, gold, and platinum different coverage cycle number were investigated to obtain the best catalytic activity towards oxygen reduction with bimetallic Pt-Au/PPAP/GCE. The optimum parameters obtained were 5.0 mmol L^{-1} *p*-aminophenol monomer concentration and 20 cycles number for polymerization. A comparison of oxygen reduction reaction using different ratios of (Au/Pt)-modified PPAP/GCE was also made (Fig. 7). The Pt deposition with 3 cycles on the $Au_{10\ cyc}$/PPAP/GCE has shown higher electrocatalytic activity towards oxygen reduction than the other modified materials. Overall results have proven that bimetallic particle-modified PPAP/GC electrodes have provided a satisfactory enhancement in peak characteristics related to oxygen reduction.

In order to investigate the effect of sodium hydroxide concentration on the reduction of oxygen, linear voltammograms were also recorded in alkaline solutions in the concentration range from 0.05 to 4.00 mol L^{-1} sodium hydroxide (Fig. 8). The peak current was decreased while the peak potential slightly shifts to positive values by the increasing of sodium hydroxide concentration. The reduction in the peak current should be mostly reasoned by the decrease in molecular oxygen solubility and diffusion coefficient besides an increase in sodium hydroxide viscosity, when sodium hydroxide concentration was changed from low concentrations to higher concentrations. The slightly positive shifting of oxygen reduction peak potential could be observed due to a strong interaction between specifically adsorbed OH^- anions at higher sodium hydroxide concentrations on the $Pt_{3\ cyc}$-$Au_{10\ cyc}$/$PPAP_{(20\ cyc)}$/GCE surface and dissolved oxygen in alkaline solution [50, 51]. The highest peak current was proved in the presence of 0.1 M sodium hydroxide solution. Therefore, 0.1 mol L^{-1} sodium hydroxide solution was chosen as optimum electrolyte for future studies.

Effect of the scan rate

In order to examine the effect of scan rate on the electrocatalytic reduction of oxygen at $Pt_{3\ cyc}$-$Au_{10\ cyc}$/$PPAP_{(20\ cyc)}$/GCE in oxygen-saturated 0.1 mol L^{-1} NaOH solutions, linear sweep voltammograms were recorded (Fig. 9a). As the scan rate increases, the electrocatalytic reduction of oxygen potential shifted negatively. The plot of the square root scan rate versus the peak current showed linear dependence in alkaline media (Fig. 9b). This situation was related to the characteristic of diffusion-controlled process at the electrode surface.

Table 1 Summary of different electrode catalysts, preparation methods, and activities of oxygen reduction reaction

Catalyst	Preparation method	Activity of oxygen reduction reaction	Reference
MHAQ/MWCNT/GCE		40 μA at −0.5 V vs. SCE in pH 7.0	[42]
Pd-modified macroporous Pt electrode	Pulse deposition	300 μA/cm^2 at 0.38 V vs. Ag/AgCl 0.1 M $HClO_4$	[43]
Au nanoparticles	Thermal citrate reduction	23 μA at 0.05 V vs. Ag/AgCl in 0.1 M sulfuric acid	[44]
Pt wire electrode		312 μA at −0.094 V vs SHE in 0.5 M KOH	[45]
$NiCo_2O_4$/N-rGO	Physical adsorption and pyrolyzation	−0.5 V vs. SCE for CoPc and −0.3 V vs. SCE for FePc in 0.1 M NaOH	[46]
Pt-Ru/C	Chemical reduction	0.75 V vs. Ag/AgCl in 0.1 M NaOH	[47]
DIHAQ on PPy/GCE	Potentiostatic method	20 μA −0.390 V vs. Ag/AgCl in pH 6.0 buffer solution	[48]
Ag/B-MWCNT	Chemical reduction	−0.45 V vs. SCE vs. in 0.1 M KOH	[49]
Pt-Au/PPAP/GCE	Electrochemical deposition with cyclic voltammetry	90 μA peak height or 1250 μA/cm^2 −0.37 V vs. Ag/AgCl in 0.1 M NaOH	Present work

MHAQ/MWCNT/GCE monohydroxy-anthraquinone/multiwall carbon nanotube-modified glassy carbon electrode, *$NiCo_2O_4$/N-rGO* $NiCo_2O_4$/N-doped reduced graphene oxide, *DIHAQ on PPy/GCE* dihydroxy 9,10-anthraquinone incorporated in polypyrrole-modified glassy carbon electrode, *Ag/B-MWCNT* Ag nanoparticles supported on boron-doped multi-walled carbon nanotubes

Rotating disc electrode voltammetric studies

The oxygen reduction kinetics were studied on $Pt_{3\ cyc}$-$Au_{10\ cyc}$/$PPAP_{(20\ cyc)}$/GCE in 0.1 mol L^{-1} sodium hydroxide, and a stable, well-defined current density-potential curves for oxygen reduction was obtained (Fig. 10). The oxygen reduction current density at different potentials varied linearly with $\omega^{-1/2}$ (Fig. 11). The linearity indicated the first-order kinetics with regard to the molecular oxygen. The electron number was estimated from the slope of Koutecký-Levich (K-L) plots for the oxygen reaction mechanism.

The K-L plots can be expressed as follows [52, 53]:

$$\frac{1}{j} = \frac{1}{j_k} + \frac{1}{B\omega^{1/2}} \tag{2}$$

where j is the measured current density, j_k is the kinetic current density, ω is the rotation rate of the electrode, and B is the Levich slope. The theoretical value can be explained by Eq. (3):

$$B = 0.62nFC(O_2)D_{O_2}^{2/3}\gamma^{-1/6} \tag{3}$$

where n is the number of electrons transferred for per oxygen molecule, F is Faraday constant (96,500 C mol^{-1}), C_{O_2} is the concentration of oxygen (1.13×10^{-6} mol cm^{-3}), D_{O_2} is the diffusion coefficient of oxygen (2.22×10^{-5} cm s^{-1}), and γ is the kinematic viscosity of the solution (1.1×10^{-2} cm s^{-1}). These coefficient values were referred to a 0.1 mol L^{-1} NaOH solution [54].

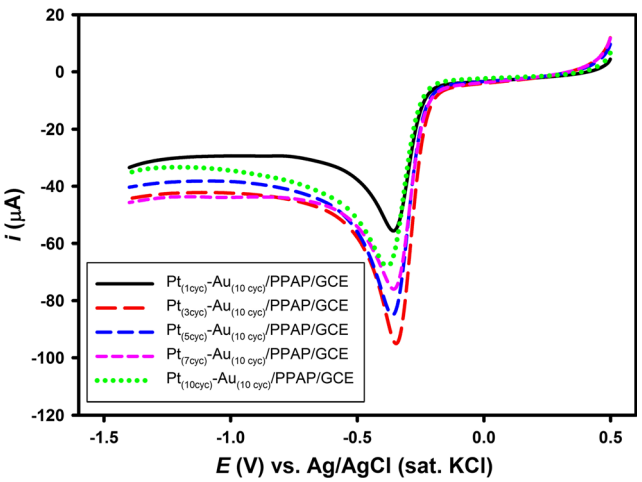

Fig. 7 Linear voltammograms for oxygen reduction at different cycle numbers of gold and platinum particle deposition on PPAP/GCE in O_2 saturated 0.1 mol L^{-1} NaOH with 50.0 mV s^{-1}

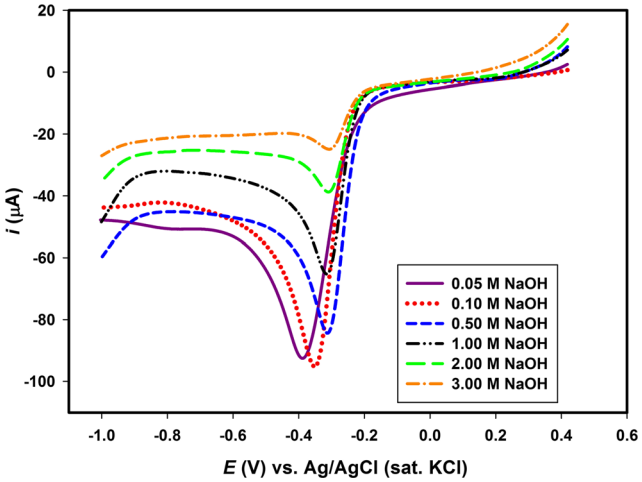

Fig. 8 Linear voltammograms for oxygen reduction on $Pt_{3\ cyc}$-$Au_{10\ cyc}$/$PPAP_{(20\ cyc)}$/GC electrode at different NaOH concentrations in O_2 saturated with 50.0 mV s^{-1}

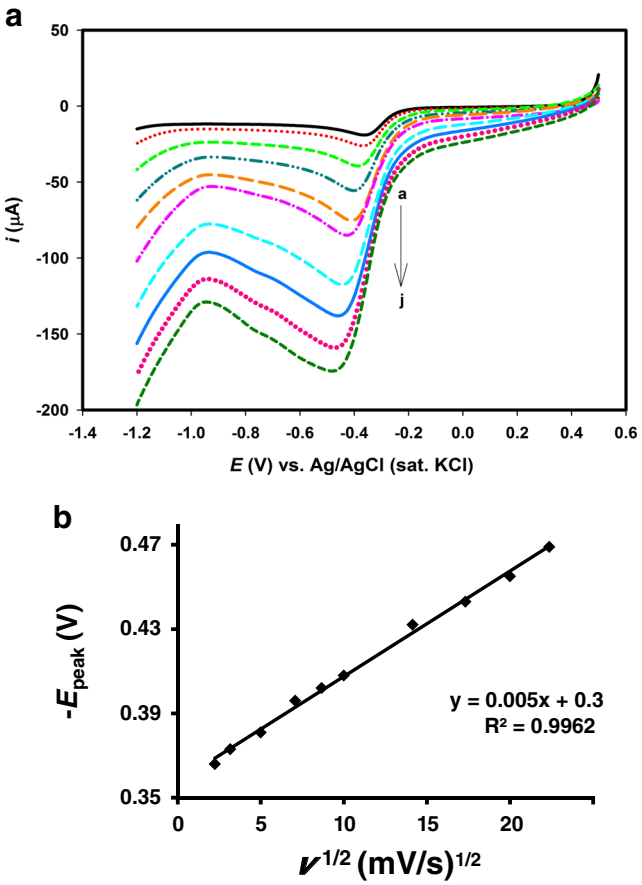

Fig. 9 **a** Linear voltammograms of $Pt_{3\ cyc}$-$Au_{10\ cyc}$/$PPAP_{(20\ cyc)}$/GCE in an O_2-saturated 0.1 mol L^{-1} NaOH solution at various scan rates: **a** 5, **b** 10, **c** 25, **d** 50, **e** 75, **f** 100, **g** 200, **h** 300, **i** 400, and **j** 500 mV s^{-1}. **b** The correlation of the reduction peak potential with the square root of the scan rate

The number of electrons transferred per oxygen molecule in oxygen reduction on the $Pt_{3\ cyc}$-$Au_{10\ cyc}$/$PPAP_{(20\ cyc)}$/GCE electrode was calculated as 3.7 from the slope of the K-L plots

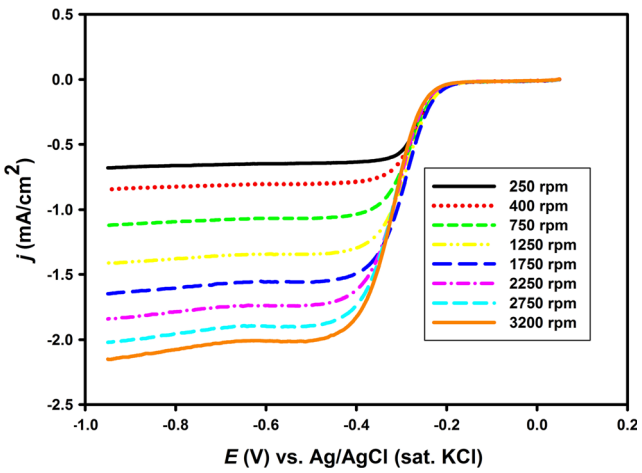

Fig. 10 Hydrodynamic voltammograms for the O_2 reduction reaction at a rotating $Pt_{3\ cyc}$-$Au_{10\ cyc}$/$PPAP_{(20\ cyc)}$/GCE in 0.1 mol L^{-1} NaOH under an O_2 atmosphere. The RDE current-potential curve was obtained at 0.01 V s^{-1} scan rate

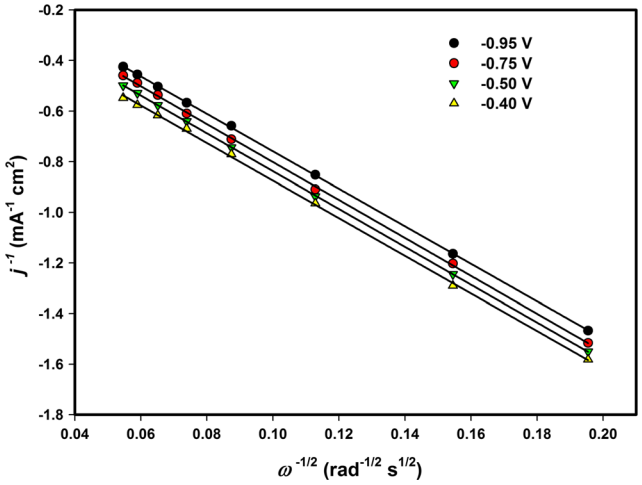

Fig. 11 Koutecky-Levich plots for O_2 reduction at different potentials on $Pt_{3\ cyc}$-$Au_{10\ cyc}$/$PPAP_{(20\ cyc)}$/GCE in 0.1 mol L^{-1} NaOH

over the whole range of potentials. This value indicates that molecular oxygen was reduced directly at almost four-electron pathway to produce water.

Stability of Pt-Au/PPAP/GCE

The long-term storage stability of the Pt-Au/PPAP/GCE was tested by taking the response of the modified electrode towards O_2 reduction. The prepared $Pt_{3\ cyc}$-$Au_{10\ cyc}$/PPAP (20 cyc)/GCE was stored in 0.1 mol L^{-1} NaOH at room temperature when not in use.

The long-term storage stability of the $Pt_{3\ cyc}$-$Au_{10\ cyc}$/$PPAP_{(20\ cyc)}$/GCE was monitored in the reduction peak of oxygen maintained as 89.12 % of the original peak current value after 25 days. Therefore, the electrode could be used for almost 4 weeks without any significant error. From the results, the $Pt_{3\ cyc}$-$Au_{10\ cyc}$/$PPAP_{(20\ cyc)}$/GCE is promising as a cathode catalyst in fuel cell applications with fine long-term storage stability.

Conclusions

A new electrocatalyst was developed as a working electrode composed of Pt-Au bimetallic particles which were homogenously distributed into PAP film by cyclic voltammetry. XPS and EDX results revealed the presence of Pt and Au on the PPAP surface, and TEM images showed the formation of 15–25 nm average bimetallic particle size of Pt-Au on PPAP. The XPS and TEM data also denoted an alloy formation on the Pt-Au-PPAP/GCE surface. The Pt-Au-modified PPAP/GC surface showed higher electrocatalytic activity towards oxygen reduction than bare GC and Au and Pt particle-modified PPAP/GC electrodes. The rotating disk electrode data analysis indicated that oxygen reduction takes place on

the $Pt_{3\ cyc}$-$Au_{10\ cyc}$/$PPAP_{(20\ cyc)}$/GCE followed by a four-electron pathway. As a result, it can be concluded that Pt-Au is a suitable catalyst for oxygen reduction in metal-air batteries, fuel cells, oxygen sensors, and metal corrosion applications.

Acknowledgments This work was supported by The Scientific and Technical Research Council of Turkey (TUBITAK) with 110T806 project number, EBILTEM with BIL-012 project number, and Ege University Research Funds (BAP project, 2010 FEN/075).

References

1. Silver AT, Juárez AS (2004) Mater Sci Eng B 110:268–271
2. Abdelwahab AA, Jung OS, Shim YB (2009) J Electroanal Chem 632:102–108
3. Wu G, Li N, Zhou DR, Mitsuo K, Xu BQ (2004) J Solid State Chem 177:3682–3692
4. Ding L, Qiao J, Dai X, Zhang J, Tian B (2012) Int J Hydrog Energy 37:14103–14113
5. Meng H, Jaouen F, Proietti E, Lefèvre M, Dodelet JP (2009) Electrochem Commun 11:1986–1989
6. Strbac S (2011) Electrochim Acta 56:1597–1604
7. Wang Z, Zhang Q, Kuehner D, Xu X, Ivaska A, Niu L (2008) Carbon 46:1687–1692
8. Qu D (2007) Carbon 45:1296–1301
9. Mao J, Yang L, Yu P, Wei X, Mao L (2012) Electrochem Commun 19:29–31
10. Sarapuu A, Nurmik M, Mandar H, Rosental A, Laaksonen T, Kontturi K, Schirin DJ, Tammeveski K (2008) J Electroanal Chem 612:78–86
11. Tegou A, Papadimitriou S, Kokkinidis G, Sotiropoulo S (2010) J Solid State Electrochem 14:175–184
12. Huang Q, Tao F, Zou L, Yuan T, Zou Z, Zhang H, Zhang X, Yang H (2015) Electrochim Acta 152:140–145
13. Huang JS, Zhang XG, Luo JM, Sun JY, Yang WJ (2008) J Solid State Electrochem 12:113–119
14. Zewde BW, Admassie S (2012) J Power Sources 216:502–507
15. Brussel MV, Kokkinidis G, Hubin A, Buess-Herman C (2003) Electrochim Acta 48:3909–3919
16. Vinayan BP, Jafri RI, Nagar R, Rajalakshmi N, Sethupathi K, Ramaprabhu S (2012) Int J Hydrog Energy 37:412–421
17. Li Q, Wu L, Wu G, Su D, Lv H, Zhang S, Zhu W, Casimir A, Zhu H, Mendoza-Garcia A, Sun S (2015) Nano Lett 15:2468–2473
18. Yang CC, Chen HR, Lee CL (2015) J Solid State Electrochem 19: 663–670
19. Qiu Y, Yu J, Wu W, Yin J, Bai X (2013) J Solid State Electrochem 17:565–573
20. Milla'n WM, Thompson TT, Arriaga LG, Smita MA (2009) Int J Hydrogen Energy 34:694–702
21. Ji Y, Li Z, Wang Z, Xu G, Yu X (2010) Int J Hydrog Energy 35: 8117–8121
22. Wu J, Zhang D, Wang Y, Wan Y (2012) Electrochim Acta 75:305–310
23. Godı'nez-Salomo'n F, Hallen-Lo'pez M, Solorza-Feria O (2012) Int J Hydrogen Energy 37:14902–14910
24. Shao M, Sasaki K, Marinkovic NS, Zhang L, Adzic RR (2007) Electrochem Commun 9:2848–2853
25. Çiftci A, Michel Ligthart DAC, Pastorino P, Hensen EJM (2013) Appl Catal B 130–131:325–335
26. Dursun Z, Karabiberoglu ŞU, Gelmez B, Ertaş FN (2011) Turk J Chem 35:513–521
27. Cui HF, Ye JS, Zhang WD, Wang J, Sheu FS (2005) J Electroanal Chem 577:295–302
28. Lee K, Zhang L, Lui H, Hui R, Shi Z, Zhang J (2009) Electrochim Acta 54:4704–4711
29. Gopalan AI, Lee KP, Manesh KM, Santhosh P, Kim JH (2006) J Mol Catal A Chem 256:335–345
30. Shan J, Pickup P (2000) Electrochim Acta 46:119–125
31. Kumar SA, Chen SM (2007) J Mol Catal A Chem Chemical 278: 244–250
32. Rı'os E, Abarca S, Daccarett P, Cong HN, Martel D, Marcoc JF, Gancedoc JR, Gautier JM (2008) Int J Hydrogen Energy 33:4945–4954
33. Liu LP, Yin ZJ, Yang ZS (2010) Bioelectrochem 79:84–89
34. Bakır ÇC, Dursun Z (2013) J Electroanal Chem 694:94–103
35. Bai J, Ndamanisha JC, Liu L, Yang L, Guo, L (2010) J Solid State Electrochem (2010) 14:2251–2256
36. Song MJ, Hwang SW, Whang D (2010) Talanta 80:1648–1652
37. Konopka SJ, McDuffie B (1970) Anal Chem 42:1741–1746
38. Guo S, Zhu Q, Yang B, Wang J, Ye B (2011) Food Chem 129: 1311–1314
39. Oztekin Y, Tok M, Bilici E, Mikoliunaite L, Yazicigil Z, Ramanaviciene A (2012) Electrochim Acta 76:201–207
40. Wen W, Zhao DM, Zhang XH, Xiong HY, Wang DF, Chen W, Zhao YD (2012) Sens Actuators B Chem 174:202–209
41. Bakır ÇC, Şahin N, Polat R, Dursun Z (2011) J Electroanal Chem 662:275–280
42. Gong Z, Zhang G, Wang S (2013) J Chem 2013:1–9
43. Du Y, Lv K, Su B, Zhang N, Wang C (2009) J Appl Electrochem 39:2409–2414
44. Jeyabharathi C, Hasse U, Ahrens P, Scholz F (2014) J Solid State Electrochem 18:3299–3306
45. Yan WY, Zheng SL, Jin W, Peng Z, Wang SN, Du H, Zhang Y (2015) J Electroanal Chem 741:100–108
46. Zhang H, Li H, Wang H, He K, Wang S, Tang Y, Chen J (2015) J Power Sources 280:640–648
47. Hosseini MG, Zardari P (2015) Applied Surface Science 345:223–231
48. Valarselvana S, Manisankar P (2011) Electrochim Acta 56:6945–6953
49. Cheng Y, Tian Y, Tsang SW, Yan C (2015) Electrochim Acta 174: 919–924
50. Zhang C, Fan Fu-Ren F, and Bard AJ (2009) J Am Chem Soc 131: 177–181
51. Dursun Z,Karabiberoglu ŞU, Gelmez B, Ertaş FN (2011) Catal Lett (2009) 132:127–132
52. Erikson H, Kasikov A, Johans C, Kontturi K, Tammeveski K, Sarapuu A (2011) J Electroanal Chem 652:1–7
53. Mamuru SA, Ozoemena KI, Fukuda T, Kobayashi N, Nyokong T (2010) Electrochim Acta 55:6367–6375
54. Elezovic NR, Babic BM, Vracar LJM, Krstajic V (2007) J Serb Chem Soc 72:699–708